Oxygen-modified Supra-nanometer-sized RuPt for Robust Alkaline HER/HOR

Youpeng Cao,[a]# Hongling Liu,[a]# Yuxuan Xiao,[a] Lun Li,[a] Jiao Yang,[a] Chunfa Liu,[a] Chengcheng Zhong,[a] Wendi Zhang,[a] Shuyang Peng,[a] Junge Yang,[a] Zhichao Yu,[a] Weng Fai Ip[b], and Hui Pan [a][b]*

[a] Institute of Applied Physics and Materials Engineering, University of Macau, Macao SAR, 999078, China

[b] Department of Physics and Chemistry, Faculty of Science and Technology, University of Macau, Macao SAR, 999078, China

# Equal contribution.

* Corresponding author.

Hui Pan: huipan@um.edu.mo (e-mail), +853 88224427 (tel.)

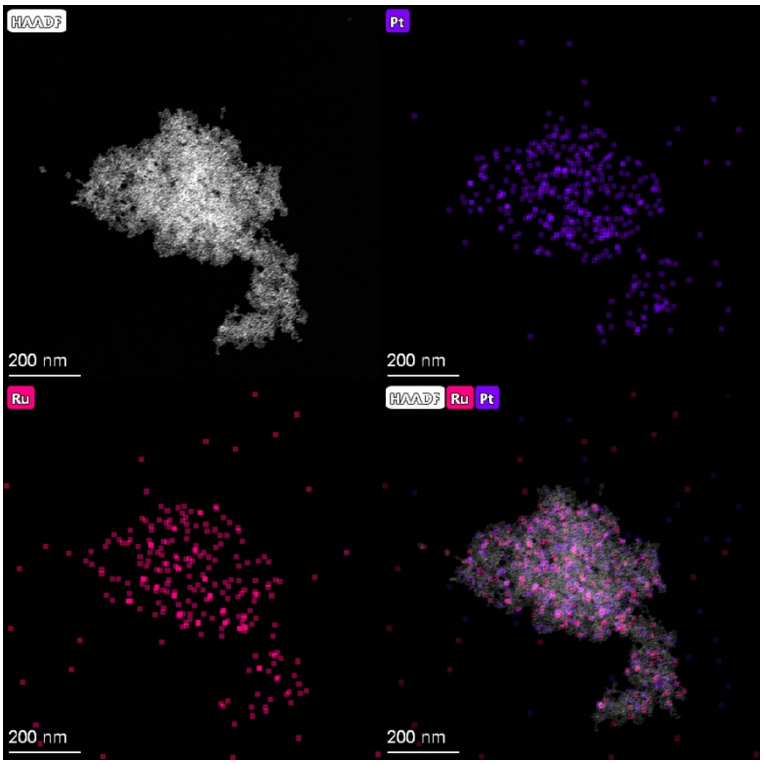

Fig. S1 The EDS mapping of RuPt.

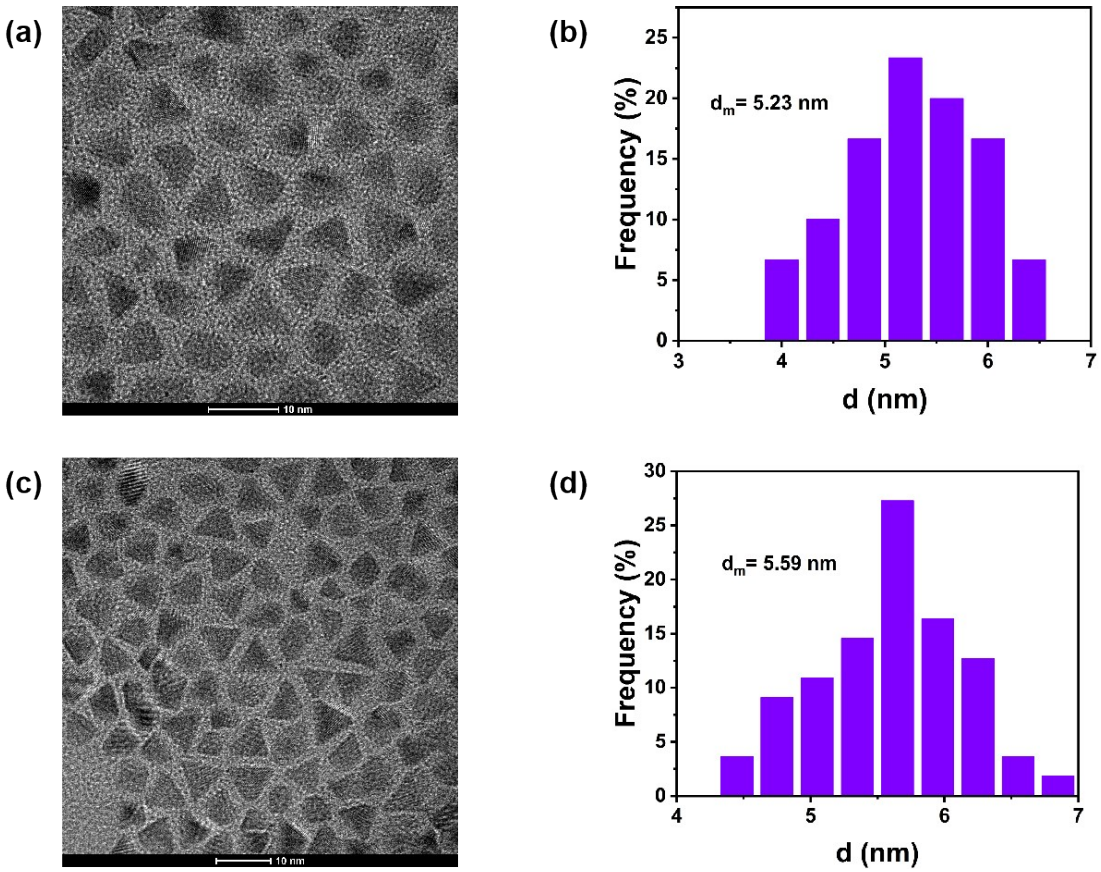

Fig. S2 (a) TEM image and (b) corresponding size distribution diagram of supra-nanometer-sized RuPt nanocrystals synthesized with a reaction time of 0.5 h. (c) TEM image and (d) corresponding size distribution diagram of supra-nanometer-sized RuPt nanocrystals synthesized with a reaction time of 1.5 h.

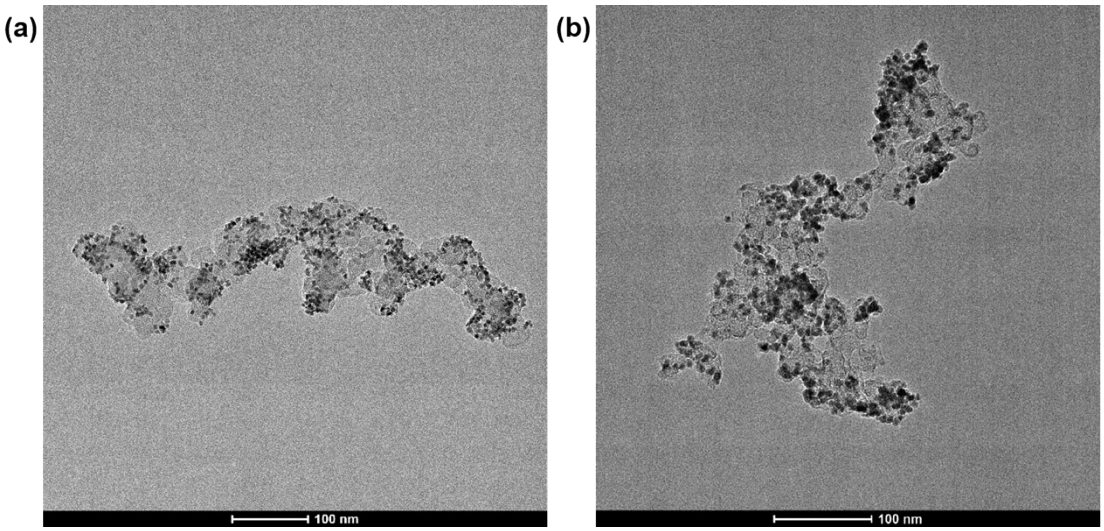

Fig. S3 TEM images of (a) RuPt/C-180 and (b) RuPt/C-220.

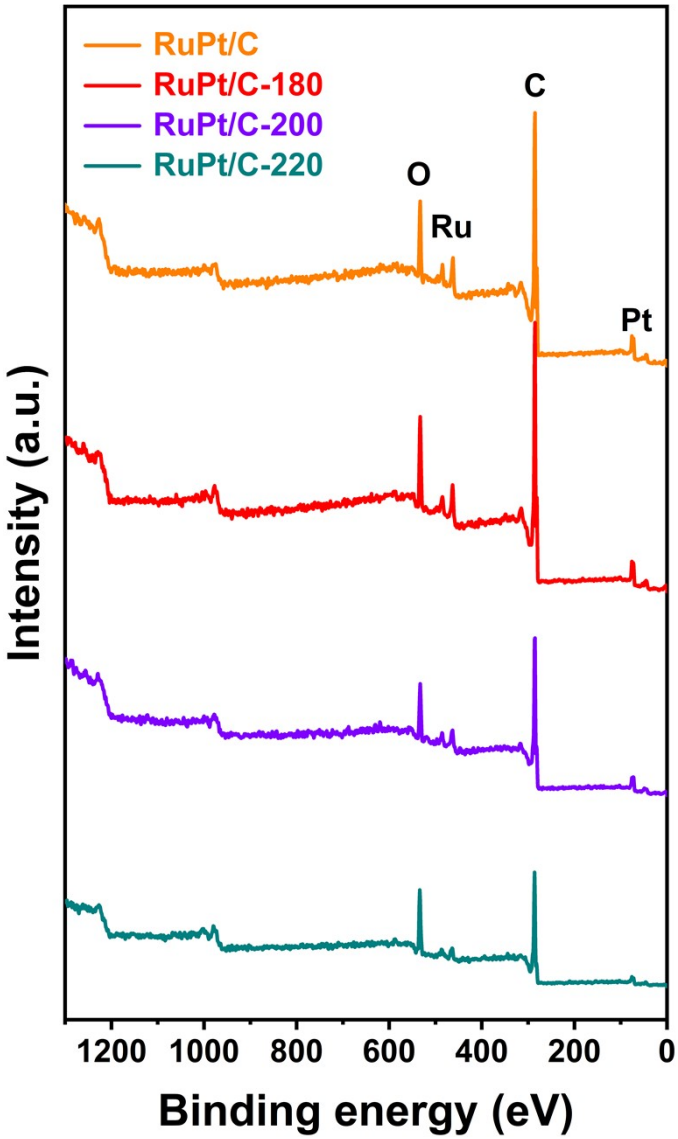

Fig. S4 XPS full spectra of RuPt/C, RuPt/C-180, RuPt/C-200, and RuPt/C-220.

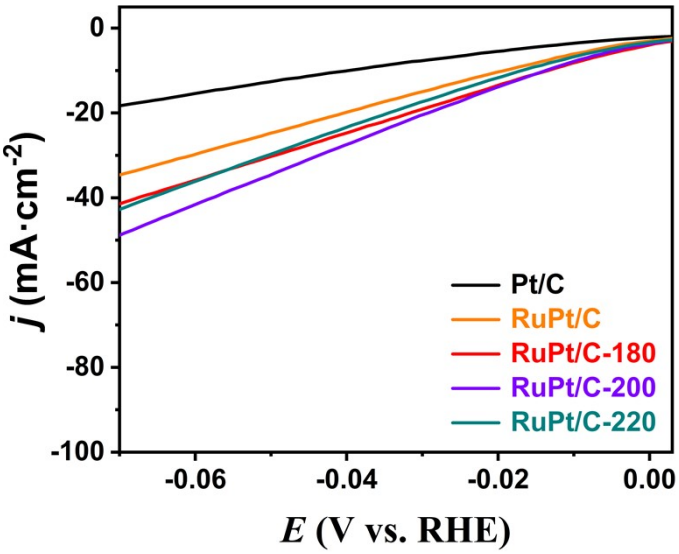

Fig. S5 HER polarization curves of commercial Pt/C, RuPt/C, RuPt/C-180, RuPt/C-200, and RuPt/C-220 without *iR* correction in a N_2-saturated 1 M KOH electrolyte with a rotating speed of 1,600 rpm.

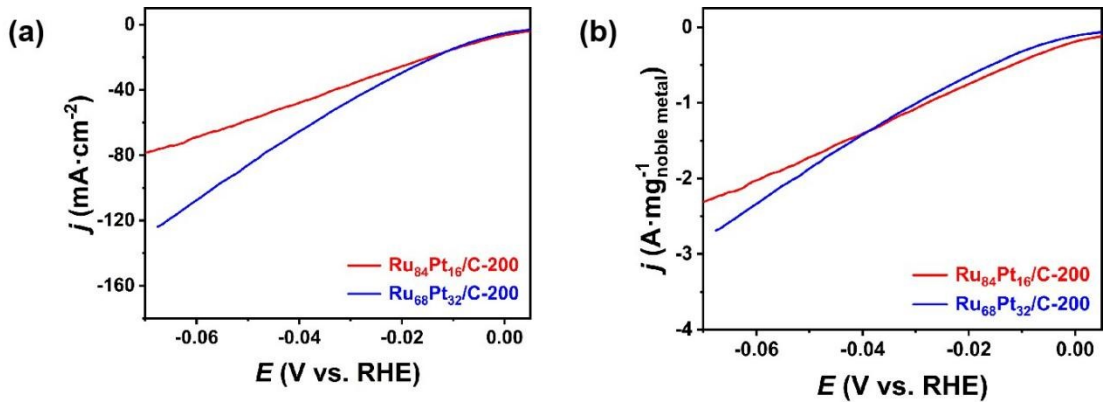

Fig. S6 (a) HER polarization curves of $Ru_{84}Pt_{16}$/C-200 (with less Pt) and $Ru_{68}Pt_{32}$/C-200 (with less Ru) in a N_2-saturated 1 M KOH electrolyte with a rotating speed of 1,600 rpm. (b) Corresponding Mass-normalized HER polarization curves in (a).

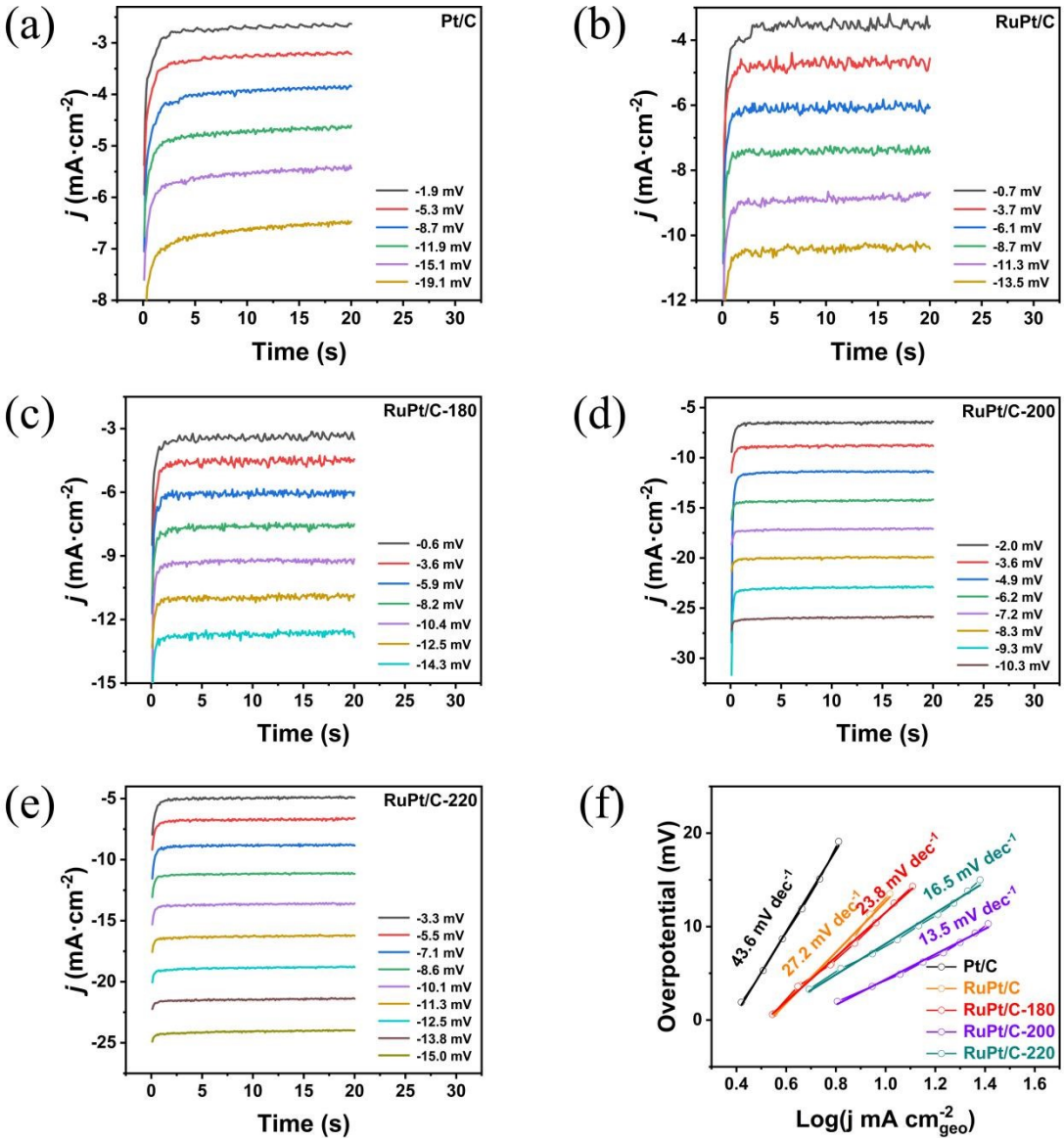

Fig. S7 Chronoamperometry study of (a) Pt/C, (b) RuPt/C, (c) RuPt/C-180, (d) RuPt/C-200 and (e) RuPt/C-220 at different applied potentials vs RHE for the HER in 1 M KOH solution (f) Tafel slopes derived from (a), (b), (c), (d) and (e).

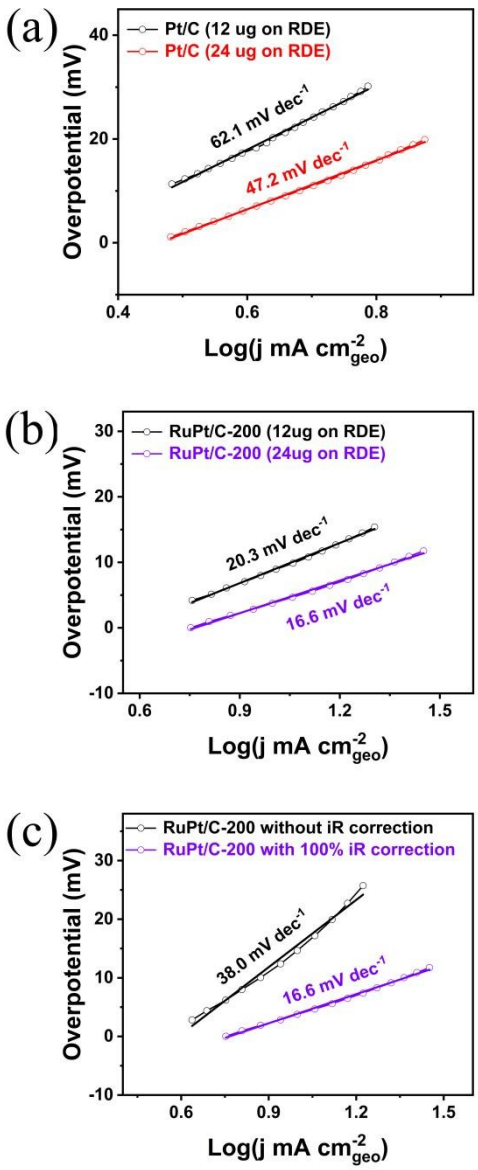

Fig. S8 (a) Tafel slopes of 12 μg and 24 μg Pt/C tested on a 0.196 cm² rotating disk electrode. (b) Tafel slopes of 12 μg and 24 μg RuPt/C-200 tested on a 0.196 cm² rotating disk electrode.(c) Tafel slopes of RuPt/C-200 (24 μg on a 0.196 cm² rotating disk electrode) catalyst without *iR* potential compensation and with 100% *iR* potential compensation. (The Tafel slope is calculated from the LSV curve unless otherwise specified.)

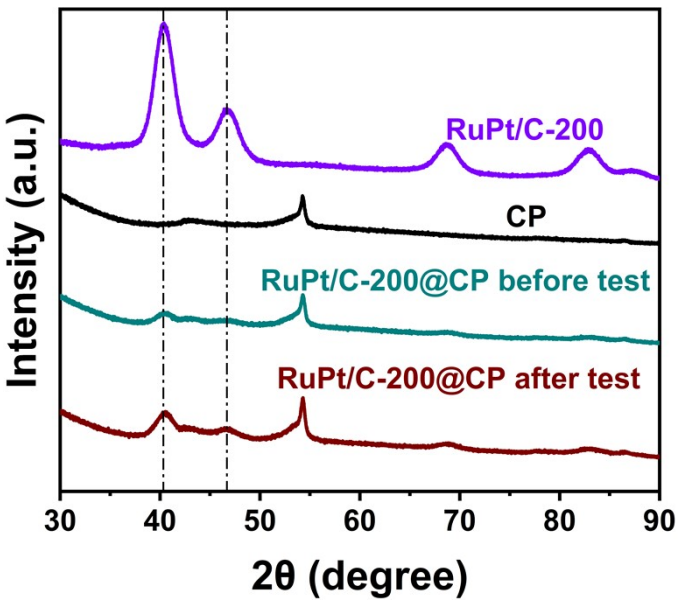

Fig. S9 XRD patterns of RuPt/C-200, CP, RuPt/C-200@CP before and after stability test.

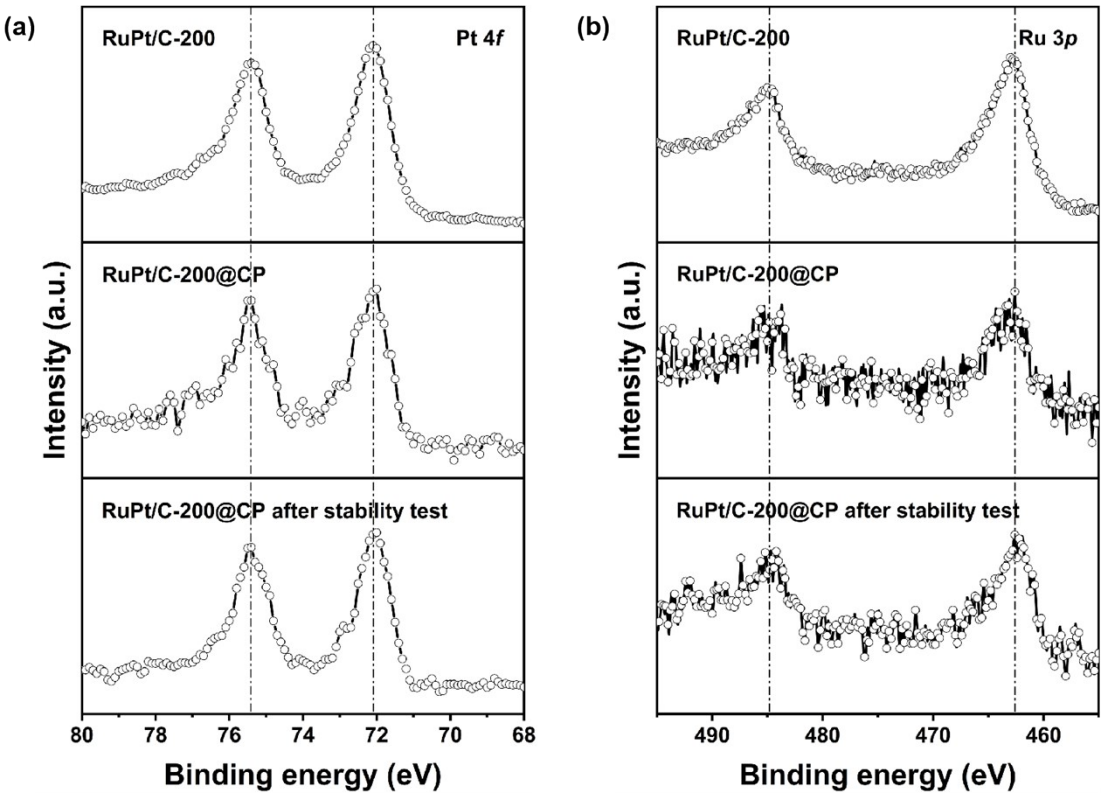

Fig. S10 High-resolution XPS spectra of (a) Pt 4f and (b) Ru 3p RuPt/C-200, RuPt/C-200@CP before and after stability test.

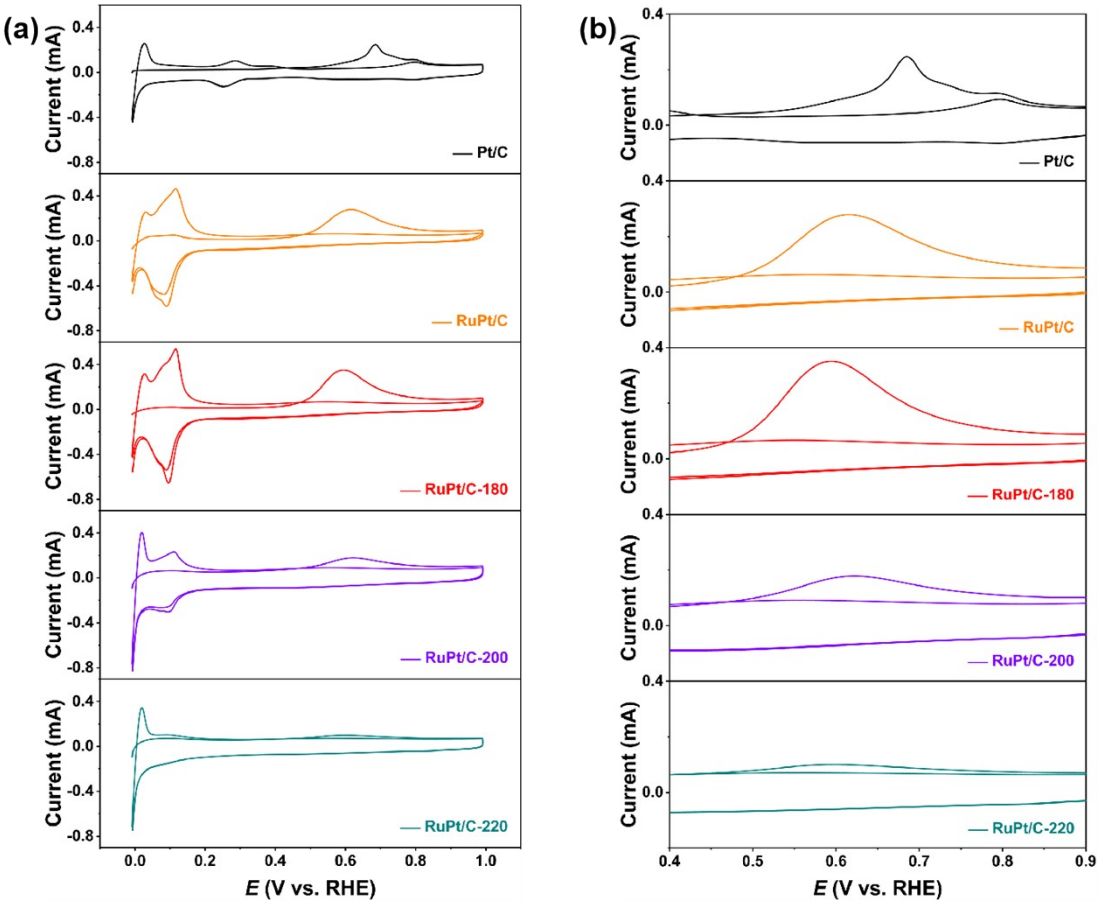

Fig. S11 (a) original and (b) magnified CO-stripping voltammograms of commercial Pt/C, RuPt/C, RuPt/C-180, RuPt/C-200, and RuPt/C-220.

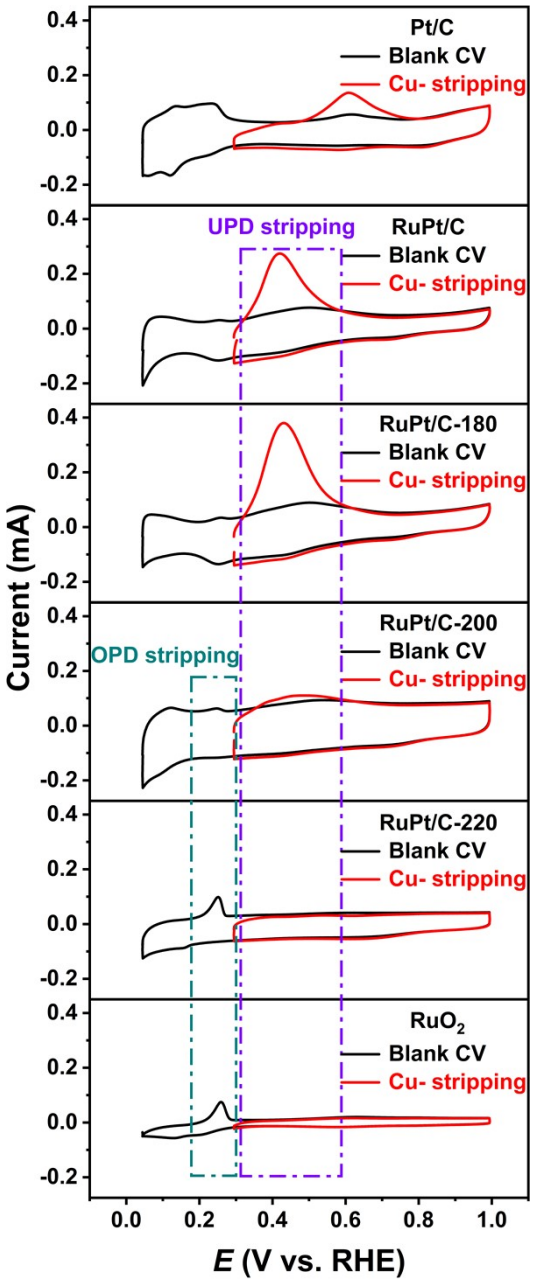

Fig. S12 CVs and Cu-stripping voltammograms of commercial Pt/C, RuPt/C, RuPt/C-180, RuPt/C-200, RuPt/C-220 and RuO_2 catalysts (loading amount: 122.4 ug cm^{-2}).

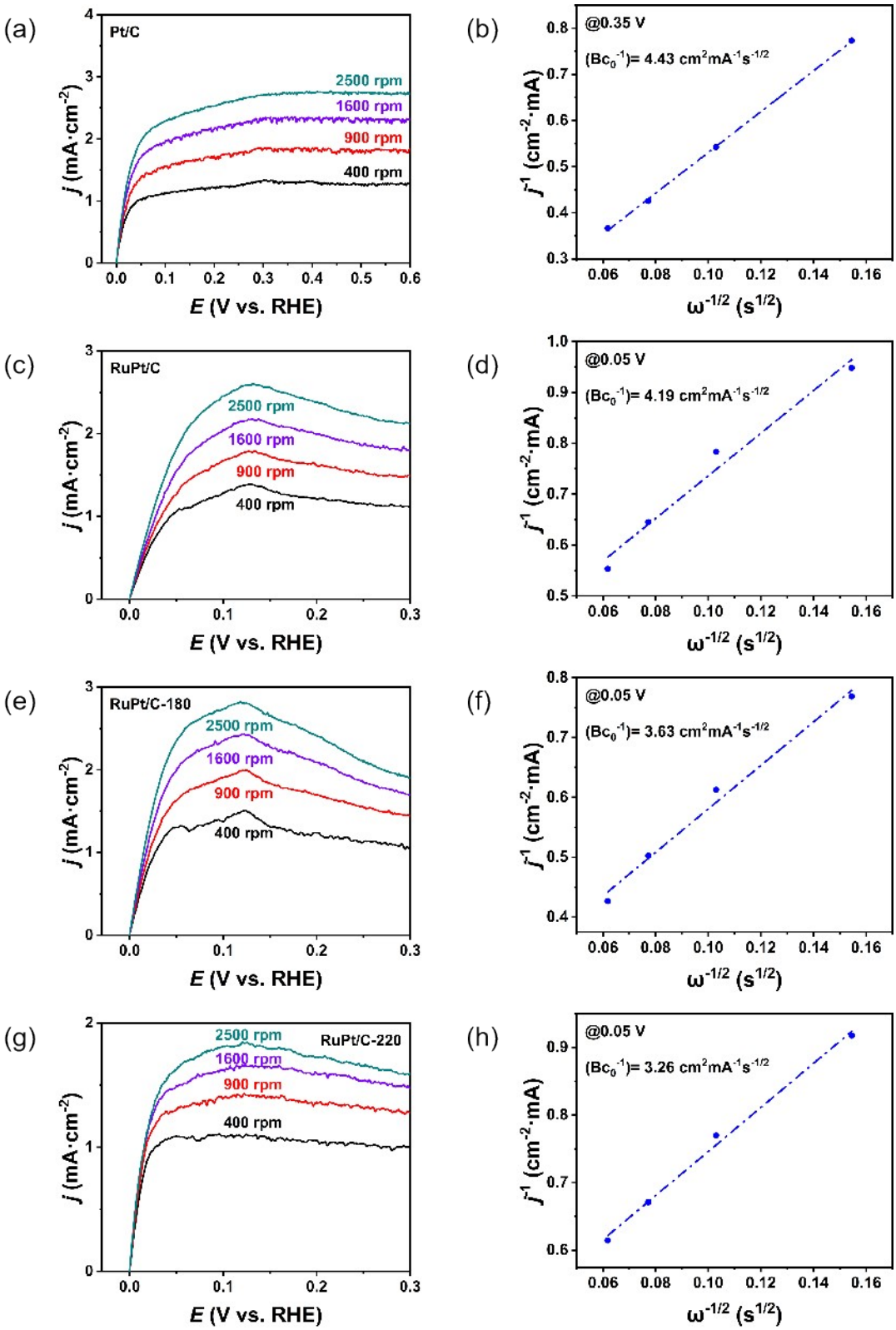

Fig. S13 HOR polarization curves and corresponding Koutechy-Levich plots of (a, b) Pt/C, (c, d) RuPt/C, (e,f) RuPt/C-180, and (g, h) RuPt/C-220 at different rotation speeds in an H_2-saturated 0.1 M KOH solution with a scan rate of 5 mV s^{-1}. The BC_0

values were derived from the Koutecky-Levich equation $\frac{1}{j} = \frac{1}{j_k} + \frac{1}{BC_0\omega^{\frac{1}{2}}}$, where ω is the rotation rate, and BC_0 is a constant related to the number of electrons transferred in a reaction, the gas concentration and diffusivity, and the electrolyte kinematic viscosity.

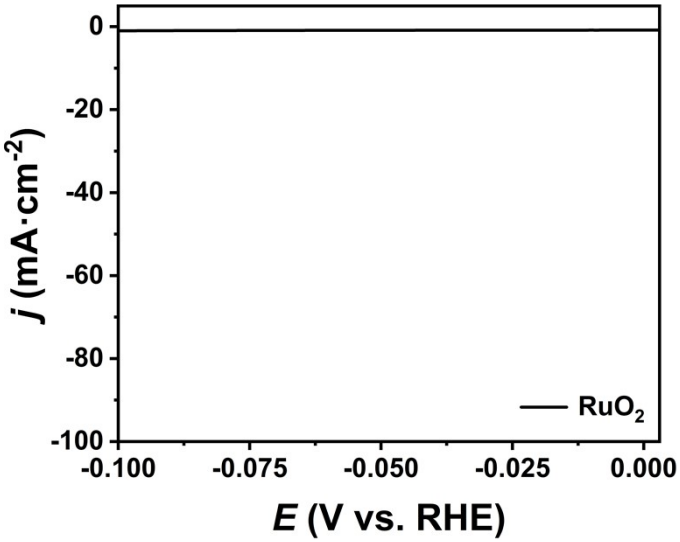

Fig. S14 HER polarization curves of commercial RuO_2 with 95% *iR* correction in a N_2-saturated 1 M KOH electrolyte with a rotating speed of 1,600 rpm.

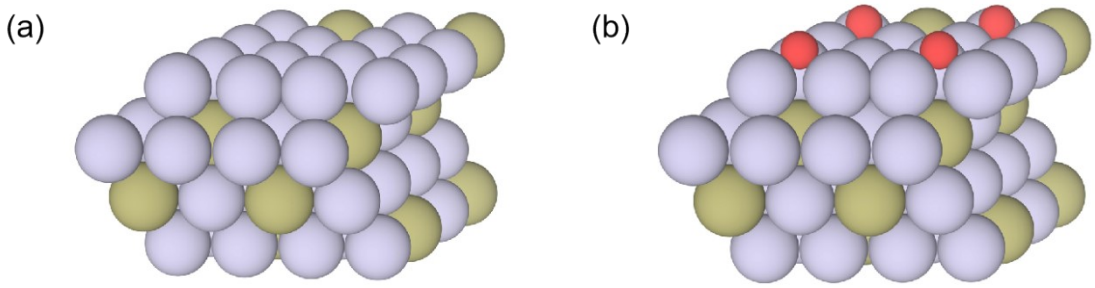

Fig. S15 The Optimized configurations of (a) pristine RuPt (111) surface and (b) partially oxidized RuPt (111).

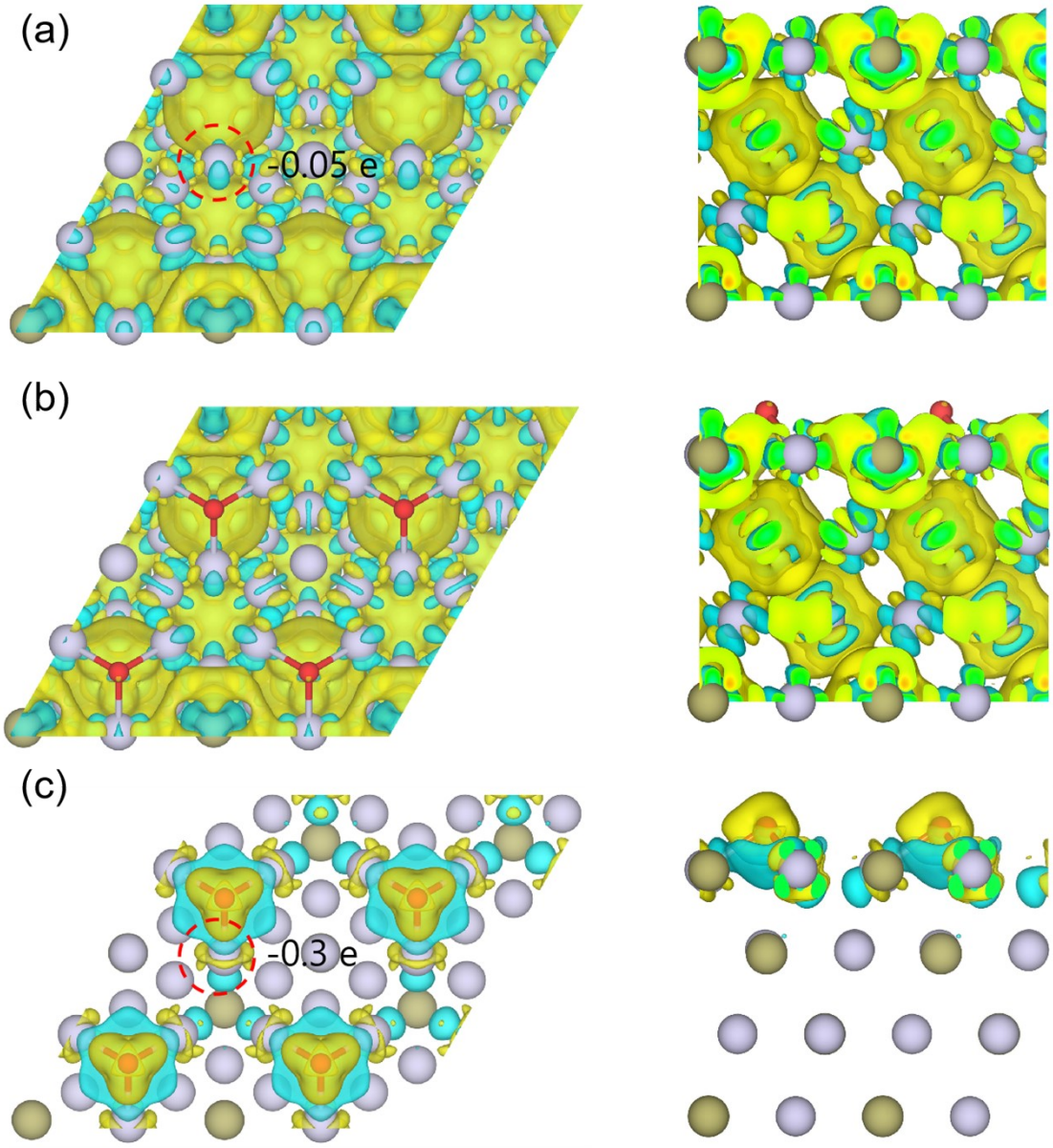

Fig. S16 The top (left) and side (right) view of differential charge density between Pt and Ru for (a) RuPt ($\Delta\rho_1$(RuPt) = ρ(RuPt) - ρ(Ru) - ρ(Pt)) and (b) oxidized RuPt ($\Delta\rho_2$(O-RuPt) = ρ(O-RuPt) - ρ(O-Ru) - ρ(Pt)). (c) Differential charge density between O and Ru for oxidized RuPt ($\Delta\rho_3$(O-RuPt) = ρ(O-RuPt) - ρ(O) - ρ(RuPt)). The value of isosurface is 0.004 eV A^{-3}. The cyan and yellow clouds represent electron depletion and accumulation, respectively. The values in the figure represent the number of loss electrons from Ru atoms.

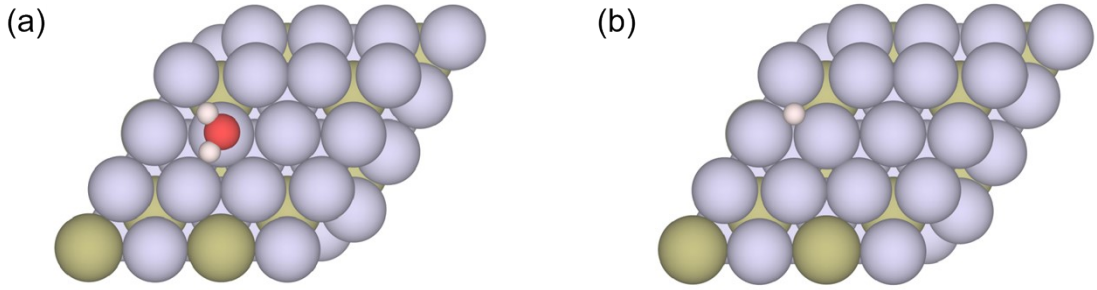

Fig. S17 Optimized atomic structure of RuPt with (a) H_2O adsorption, (b) *H adsorption on RuPt.

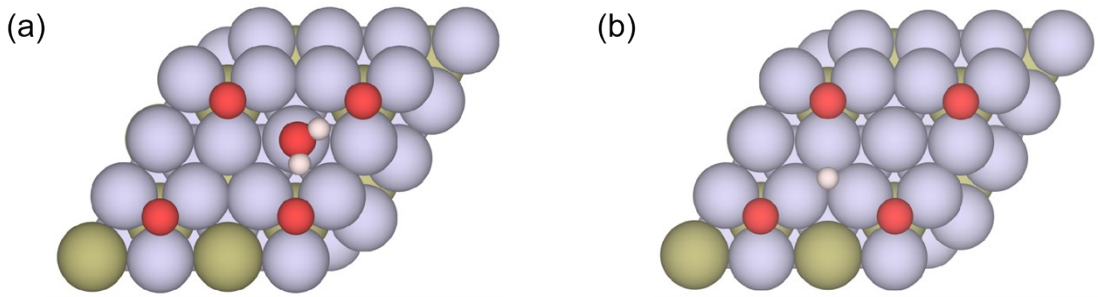

Fig. S18 Optimized atomic structure of (a) H_2O adsorption, (b) *H adsorption on oxidized RuPt.

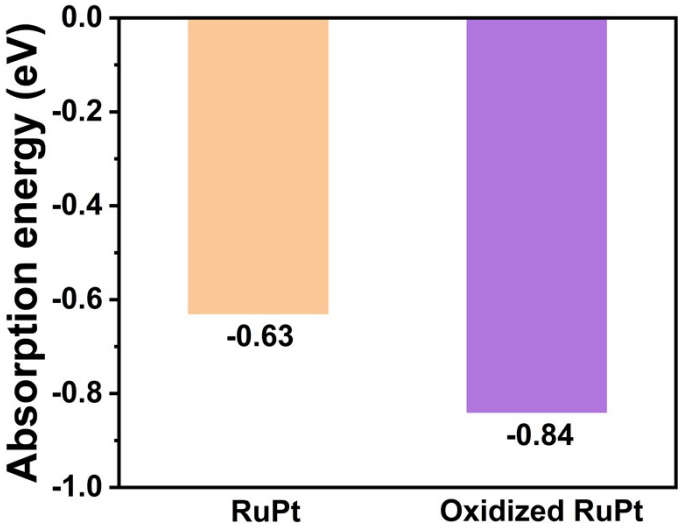

Fig. S19 Adsorption energies of water on pristine RuPt and oxidized RuPt.

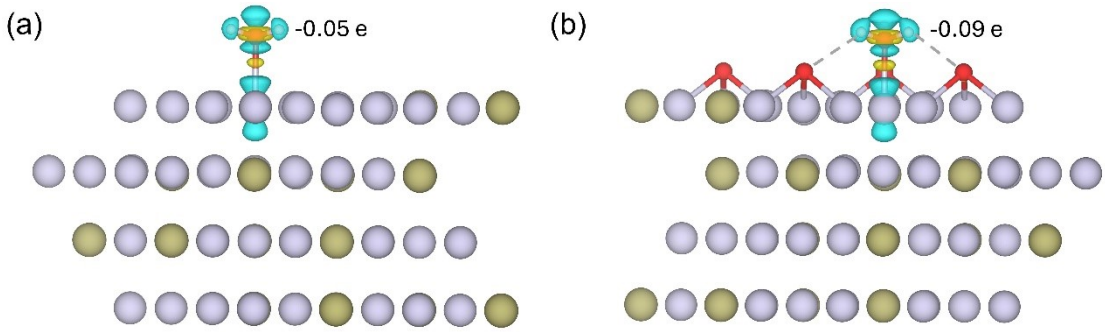

Fig. S20 Differential charge density between H_2O and (a) RuPt, (b) oxidized RuPt. The dotted line represents the hydrogen bond between H in H_2O and surface O. The value of isosurface is 0.004 eV A^{-3}. The cyan and yellow clouds represent electron depletion and accumulation, respectively. The values in the figure represent the number of donated electrons from H_2O.

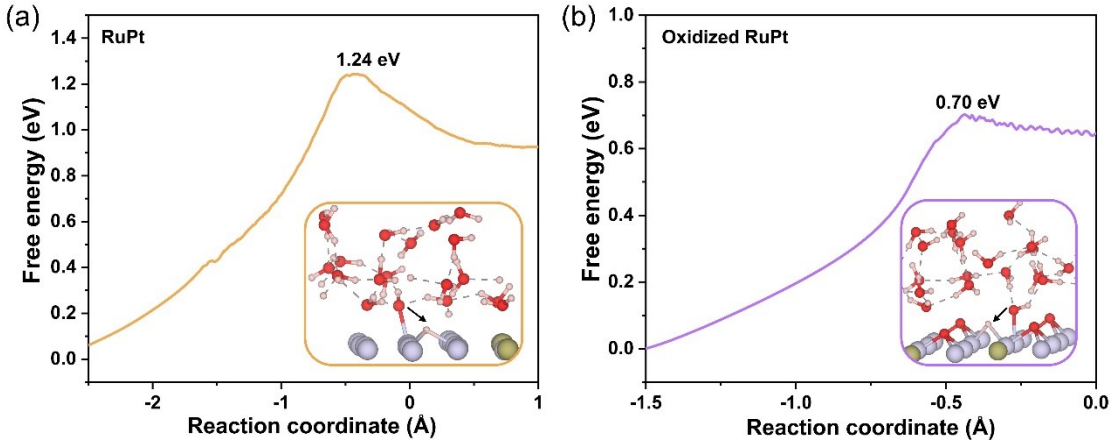

Fig. S21 The kinetic barrier for H_2O dissociation to *H and *OH on (a) RuPt and (b) oxidized RuPt. The insets are the snapshots of the transition states.

Table S1. The Pt/Ru molar ratio of the corresponding nanocrystals determined by ICP-MS.

Samples	Pt (at.%)	Ru (at.%)
RuPt/C	20.81	79.19
RuPt/C-180	20.90	79.10
RuPt/C-200	20.94	79.06
RuPt/C-220	20.93	79.07
$Ru_{84}Pt_{16}$/C-200 (with less Pt)	16.28	83.72
$Ru_{68}Pt_{32}$/C-200 (with less Ru)	31.73	68.27

Table S2. The values of 2θ(°), lattice spacing (d) and derived lattice strain (s) of Pt (111) (JCPDS no. 04-0802), RuPt/C, RuPt/C-180, RuPt/C-200 and RuPt/C-220.

Samples	2θ(°)	d	s
Pt (111) (JCPDS no. 04-0802)	39.763	2.2650	0
RuPt/C	40.475	2.2268	1.69%
RuPt/C-180	40.435	2.2287	1.60%
RuPt/C-200	40.405	2.2305	1.52%
RuPt/C-220	40.427	2.2293	1.58%

According to a previous definition, the lattice strain of Pt (111) can be obtained by the following equation[1]:

$$s = \frac{d_n - d_b}{d_b} \times 100\%$$

Where d_b is the lattice spacing of bulk Pt (that is, 0.2265; JCPDS no. 04-0802), and d_n is the lattice spacing of the corresponding RuPt nanocrystals. A positive value of lattice strain (s) represents tensile strain, while a negative value represents compressive strain.

Table S3. The results of deconvolution of the Ru $3d_{3/2}$, Pt $4f$ and O1s XPS spectra of different catalysts.

	Ru $3d_{5/2}$		Pt $4f$	O $1s$	
	BE/eV	Atomic Ratio (to Ru^0)	BE/eV	BE/eV	Area Ratio (to O_L)
RuPt/C	280.58	1	72.21	530.72 (O_{Lat})	1
	281.15	1.35		532.84 (O_V)	10
				534.28 (O_{Abs})	5.8
RuPt/C-180	280.56	1	72.13	530.51 (O_{Lat})	1
	281.31	1.34		532.89 (O_V)	4.35
				534.32 (O_{Abs})	2.09
RuPt/C-200	280.53	1	72.02	530.48 (O_{Lat})	1
	281.21	2.14		532.79 (O_V)	3.13
				534.25 (O_{Abs})	1.41
RuPt/C-220	280.51	1	71.99	530.05 (O_{Lat})	1
	281.35	5.80		532.80 (O_V)	0.65
				534.46 (O_{Abs})	4.35

Table S4. Comparison of impedance of different catalysts.

Samples	R_s (ohm)	R_{ct} (ohm)
Pt/C	5.61	15.3
RuPt/C	5.65	6.79
RuPt/C-180	5.51	4.73
RuPt/C-200	5.59	1.57
RuPt/C-220	5.31	2.43

Table S5. Comparison of overpotential at 10 mA cm^{-2} and Tafel plots of different catalysts for alkaline HER in 1 M KOH electrolyte.

Catalysts	η10 (mV)	Tafel slope (mV dec^{-1})	Ref.
RuPt/C-200	4.4	18.4	**This work**
Ru-CrO_x@CN	7	30.1	[2]
Ru-Ga_{SA}/N-C	5	21.1	[3]
Ru@CQDs	10	47	[4]
Ru_2P/WO_3@NPC	15	18	[5]
$RuMo_2C$@CNT	15	26	[6]
Pt-Ru/RuO_2	18	18.5	[7]
2DPC-RuMo	18	25	[8]
D-NiO-Pt	20	31.1	[9]
Pt_{SA}-Mn_3O_4	24	54	[10]
2D-Pt ND/LDH	25	32.2	[11]
Ru/np-MoS_2	30	31	[12]
CoPt-Pt_{SA}	31	43.65	[13]
Vo-Ru/HfO_2-OP	39	29	[14]
Ni_5P_4-Ru	54	52	[15]

References

1. M. C. Luo, Z. L. Zhao, Y. L. Zhang, Y. J. Sun, Y. Xing, F. Lv, Y. Yang, X. Zhang, S. Hwang, Y. N. Qin, J. Y. Ma, F. Lin, D. Su, G. Lu,S. J. Guo, *Nature*, 2019, **574**, 81-85.
2. B. Zhang, J. Wang, G. Liu, C. Weiss, D. Liu, Y. Chen, L. Xia, P. Zhou, M. Gao, Y. Liu, J. Chen, Y. Yan, M. Shao, H. Pan,W. Sun, *Nat. Catal.*, 2024, **7**, 441-451.
3. C. Zhou, J. Shi, Z. Dong, L. Zeng, Y. Chen, Y. Han, L. Li, W. Zhang, Q. Zhang, L. Gu, F. Lv, M. Luo,S. Guo, *Nat. Commun.*, 2024, **15**, 6741.
4. W. Li, Y. Liu, M. Wu, X. Feng, S. Redfern, Y. Shang, X. Yong, T. Feng, K. Wu, Z. Liu, B. Li, Z. Chen, J. Tse, S. Lu,B. Yang, *Adv. Mater.*, 2018, **30**, 1800676.
5. X. Jiang, H. Jang, S. Liu, Z. Li, M. Kim, C. Li, Q. Qin, X. Liu,J. Cho, *Angew. Chem. Int. Ed.*, 2021, **60**, 4110-4116.
6. X. Wu, Z. Wang, D. Zhang, Y. Qin, M. Wang, Y. Han, T. Zhan, B. Yang, S. Li, J. Lai,L. Wang, *Nat. Commun.*, 2021, **12**, 4018.
7. Y. Zhu, M. Klingenhof, C. Gao, T. Koketsu, G. Weiser, Y. Pi, S. Liu, L. Sui, J. Hou, J. Li, H. Jiang, L. Xu, W. Huang, C. Pao, M. Yang, Z. Hu, P. Strasser,J. Ma, *Nat. Commun.*, 2024, **15**, 1447.
8. K. Tu, D. Tranca, F. Rodríguez-Hernández, K. Jiang, S. Huang, Q. Zheng, M. Chen, C. Lu, Y. Su, Z. Chen, H. Mao, C. Yang, J. Jiang, H. Liang,X. Zhuang, *Adv. Mater.*, 2020, **32**, 2005433.
9. Y. Yan, J. Lin, T. Xu, B. Liu, K. Huang, L. Qiao, S. Liu, J. Cao, S. Jun, Y. Yamauchi,J. Qi, *Adv. Energy Mater.*, 2022, **12**, 2200434.
10. J. Wei, K. Xiao, Y. Chen, X. Guo, B. Huang,Z. Liu, *Energy Environ. Sci.*, 2022, **15**, 4592-4600.
11. Y. Hong, S. Dutta, S. Jang, O. Okello, H. Im, S. Choi, J. Han,I. Lee, *J. Am. Chem. Soc.*, 2022, **144**, 9033-9043.
12. K. Jiang, M. Luo, Z. Liu, M. Peng, D. Chen, Y. Lu, T. Chan, F. de Groot,Y. Tan, *Nat. Commun.*, 2021, **12**, 1687.
13. W. Yang, P. Cheng, Z. Li, Y. Lin, M. Li, J. Zi, H. Shi, G. Li, Z. Lian,H. Li, *Adv. Funct. Mater.*, 2022, **32**, 2205920.
14. G. Li, H. Jang, S. Liu, Z. Li, M. Kim, Q. Qin, X. Liu,J. Cho, *Nat. Commun.*, 2022, **13**, 1270.
15. Q. He, D. Tian, H. Jiang, D. Cao, S. Wei, D. Liu, P. Song, Y. Lin,L. Song, *Adv. Mater.*, 2020, **32**, 1906972.